

**DYNAMIC AXIAL AND OBLIQUE CRUSHING OF
FOAM-FILLED ALUMINIUM CONICAL TUBES**

FAUZIAH MAT

**UNIVERSITI MALAYSIA PERLIS
2015**

© This item is protected by original copyright



**DYNAMIC AXIAL AND OBLIQUE CRUSHING OF
FOAM-FILLED ALUMINIUM CONICAL TUBES**

by

**FAUZIAH MAT
(1040610531)**

A work submitted in fulfillment of the requirements for the degree of
Doctor of Philosophy

**School of Mechatronic Engineering
UNIVERSITI MALAYSIA PERLIS**

2015

THESIS DECLARATION

© This item is protected by original copyright

ACKNOWLEDGMENTS

In the name of Allah. The Most Gracious and the Most Merciful. First and foremost, I thank Allah S.W.T for being with me, guiding me and giving me the patience, strength and knowledge to complete this work.

I would like to express my deep gratitude and appreciation to my supervisors, Assoc. Prof. Dr. Khairul Azwan Ismail, Prof. Dr. Sazali Yaacob and Dr. Zaini Ahmad for their valuable supervision, continuous encouragement, inspiring suggestion and guidance in the preparation of this thesis.

The financial support of the Government of Malaysia, Ministry of Education and Universiti Malaysia Perlis (UniMAP) is greatly acknowledged.

Many thanks dedicated to Prof. W. Cantwell and the research team in School of Engineering, University of Liverpool and Prof. Dr. B.C. Tan and the research members of the Department of Mechanical Engineering, National University of Singapore for their assistance in conducting the experiments. Thanks are also due to Assoc. Prof. Dr. Qasim H. Shah of Department of Mechanical Engineering, Islamic International University of Malaysia and Prof. Dr. Mohd Nasir Tamim of Faculty of Mechanical Engineering, Universiti Teknologi Malaysia for the permission to use their labs to perform the finite element analysis. Also, Mr. Muhamad Aliff Mad Yussof, School of Mechatronic Engineering, UniMAP, Mr. Mazlan Mohd Husin, School of Manufacturing, UniMAP and all of the staff in the Centre of Postgraduate, UniMAP for their kind cooperation. To my fellow researchers especially Saidatul Ardeenawatie Awang, Jerrita Arun and Yusnita Ali for their supports and friendships.

I extend my appreciation and gratitude to my parents, loving sister and brothers for their support, love and prayers. Finally, I wish to express my deepest thank to my beloved daughter for giving me happiness, joy and enduring love. Your presence is always my strength and courage and I therefore dedicate my thesis to one and only, Iman Amani.

Fauziah Mat

2014

TABLE OF CONTENTS

THESIS DECLARATION	i
ACKNOWLEDGMENTS	ii
TABLE OF CONTENTS	iii
LIST OF TABLES	vii
LIST OF FIGURES	viii
LIST OF ABBREVIATIONS	xiii
LIST OF SYMBOLS	xiv
ABSTRAK	xvii
ABSTRACT	xviii
CHAPTER 1: INTRODUCTION	1
1.1 Introduction	1
1.2 Thin-walled tubes and foam as energy absorbers.	2
1.3 Problem statement	.5
1.4 Research objective	8
1.5 Research scopes.	9
1.6 Research hypothesis.	12
1.7 Thesis outline	13
CHAPTER 2: LITERATURE REVIEW	15
2.1 Introduction	15
2.2 Impact mechanics .	15
2.2.1 Inertia effect	16
2.2.2 Strain rate effect	16
2.3 Effectiveness of energy absorber.	.19
2.3.1 Energy absorbed	19
2.3.2 Peak force	20

2.3.3	Specific Energy Absorption (<i>SEA</i>)	21
2.4	Thin-walled tubes as energy absorbers.	.22
2.4.1	Circular tubes	23
2.4.2	Square and rectangular tubes	25
2.4.3	Tapered tubes	27
2.4.4	Conical tubes	29
2.5	Cellular materials for thin-walled tubes.	.32
2.5.1	Metallic foams	32
2.5.2	Polymeric foams	34
2.6	Foam-filled tubes	.35
2.7	Finite Element Method (FEM)	.39
2.7.1	Finite Element (FE) analysis in crashworthiness study	40
2.7.2	Explicit Finite Element (FE) code - LS-DYNA	41
2.7.3	Material model for Finite Element (FE) model development	42
2.8	Optimization on thin-walled tubes under impact loading.	44
2.8.1	Response surface method (RSM)	45
2.8.2	Empirical model for RSM	46
2.8.3	Model fitting	48
2.9	Chapter summary.	.49
CHAPTER 3: RESEARCH METHODOLOGY		50
3.1	Introduction	.50
3.2	Geometry and meshing element size	.52
3.3	Material model.	.54
3.4	Loading, interaction and boundary conditions	59
3.5	Experimental testing of empty and foam-filled tubes.	60
3.5.1	Quasi-static test	60
3.5.2	Dynamic Test: axial and oblique loading	63
3.6	Chapter summary.	.67
CHAPTER 4: FE MODEL VALIDATION		68
4.1	Introduction	.68
4.2	Experimental validation of FE model under axial loading .	.69
4.3	Experimental validation of FE model	.72

4.4	Chapter summary.	.76
CHAPTER 5: RESULTS AND DISCUSSION		78
5.1	Introduction	78
5.2	Dynamic response under axial loading.	79
5.2.1	Effect of filler density for variation of semi apical angle	80
5.2.2	Effect of filler density for variation of length	84
5.2.3	Effect of filler density for variation of diameter	88
5.2.4	Effect of filler density for variation of thickness	90
5.2.5	Effect of filler density for variations of material	93
5.2.6	Identification of critical total tube mass and critical filler density	96
5.2.7	SEA and initial peak force	102
5.3	Dynamic response under oblique loading.	107
5.3.1	Effect of filler density in dynamic oblique loading	109
5.3.2	Effect of filler density for variation of semi apical angle	111
5.3.3	Effect of filler density for variation of tube length	115
5.3.4	Effect of filler density for variation of diameter	119
5.3.5	Effect of filler density for variation of thickness	121
5.3.6	Effect of filler density for variations of materials	123
5.3.7	Identification of critical total tube mass and critical filler density	126
5.3.8	SEA and initial peak force	131
5.3.9	Chapter summary	137
CHAPTER 6: OPTIMIZATION		139
6.1	Introduction	139
6.2	Optimization for dynamic axial loading	140
6.2.1	Deterministic objective, constraints and performance function of SEA and initial peak force	140
6.2.2	Response Surface (RS) model	142
6.2.3	Single objective optimization	150
6.2.4	Multiobjective optimization	152
6.3	Optimization for dynamic oblique loading	153
6.3.1	Deterministic objective, constraints and performance function of SEA and initial peak force	154

6.3.2	Response Surface (RS) model	155
6.3.3	Single objective optimization	162
6.3.4	Multiobjective optimization	165
6.4	Summary	166
CHAPTER 7: CONCLUSIONS AND FUTURE WORK		168
7.1	Introduction	168
7.2	Conclusions	168
7.3	Contribution to knowledge	170
7.4	Suggestions for future works.	171
REFERENCES		173
APPENDIX A		184
APPENDIX B		186
APPENDIX C		188
LISTS OF PUBLICATIONS		189

LIST OF TABLES

NO	PAGE
3.1: True stress-strain data points for carbon steel.	55
3.2: Material parameters for the aluminium foam (Ahmad & Thambiratnam, 2009c).	58
5.1: Geometrical parameters for thin-walled tubes.	79
5.2 : Geometrical parameters for empty and foam-filled tubes.	109
6.1: Design matrix of initial peak force and <i>SEA</i> obtained from FE analysis for the selected design points ($V = 6$ m/s).	143
6.2: Design matrix of initial peak force and <i>SEA</i> obtained from FE analysis for the selected design points ($V = 20$ m/s).	144
6.3: Accuracy of different RS models for impact velocity of 6 m/s and 20 m/s.	146
6.4: Ideal optimums of the two single objective functions for empty and foam-filled aluminium tubes subjected to dynamic axial loading at 6 m/s and 20 m/s.	151
6.5: Optimization results of empty and foam-filled aluminium tubes.	153
6.6: Design matrix of initial peak force and <i>SEA</i> obtained from FE analysis for the selected design points ($V = 6$ m/s).	156
6.7: Design matrix of initial peak force and <i>SEA</i> obtained from FE analysis for the selected design points ($V = 20$ m/s).	157
6.8: Accuracy of different RS models for different velocities.	159
6.9: Ideal optimums of the two single objective functions for empty and foam-filled aluminium tubes subjected to oblique dynamic loading at 6 m/s and 20 m/s.	164
6.10: Optimization results of empty and foam-filled aluminium tubes.	166

LIST OF FIGURES

NO	PAGE
1.1: Total road traffic accidents in Malaysia for the year of 2012 (<i>Road Safety Situation In Malaysia</i> , 2013).	1
1.2: Introduction of Boge impact absorber to Peugeot 3008 model (Peugeot, March 2014).	4
2.1: Force versus deformation of an empty circular 6060-T5 aluminium tube under quasi-static axial loading (Guillow, Lu, & Grzebieta, 2001).	21
2.2: (a) Concertina ($D = 97.9$ mm, $t = 1.9$ mm, $L = 196$ mm) and (b) diamond ($D = 96.5$ mm, $t = 0.54$ mm, $L = 386$ mm) mode of deformations of an empty circular 6060-T5 aluminium tube under quasi-static axial loading (Guillow et al., 2001).	24
2.3: Axially crushed square tubes: (a) compact and (b) non-compact (Reddy & Al Hassani, 1993).	26
2.4: (a) Single tapered and (a) double-tapered foam-filled tubes before and after quasi-static compression (Reid & Reddy, 1986a).	28
2.5: Deformation profiles of (a) straight and (b) tapered tubes at $V=30$ m/s (Nagel & Thambiratnam, 2004).	29
2.6: Deformed profiles of empty conical carbon steel tube under quasi-static axial loading: (a) $t = 2.41$ mm (b) $t = 1.19$ mm (Ahmad & Thambiratnam, 2009b).	31
2.7: Mechanical response of ideal aluminium foam under compressive loading (Santosa & Wierzbicki, 1998).	33
2.8: Interaction effect of foam-filled tubes (Hanssen et al., 2000a).	36
2.9: Specific energy absorption for different strengthening methods (Santosa & Wierzbicki, 1998).	37
2.10: Predicted and experimental specific energy absorption vs. total mass of empty and foam-filled aluminium tubes (Güden & Kavi, 2006).	38
3.1: Flow chart of research methodology.	51
3.2: FE model of empty and foam-filled conical tubes with defined loading and boundary conditions under dynamic axial loading.	53

3.3: FE model of empty and foam-filled straight tubes with defined loading and boundary conditions under dynamic axial loading.	53
3.4: FE model of (a) straight and (b) conical tubes with defined loading and boundary conditions under dynamic oblique loading.	53
3.5: True stress strain curve of aluminium.	55
3.6: Stress strain curve for extruded polystyrene.	59
3.7: Internal and kinetic energy plot of dynamic loading.	60
3.8: Compression test of extruded polystyrene foam specimen.	61
3.9: Tensile test of aluminium specimen.	61
3.10: Schematic diagram of axes direction for foam sheet.	62
3.11: Stress-strain curves of extruded polystyrene tested in different planes.	62
3.12: Empty and foam-filled of (a) straight and (b) conical aluminium tubes.	64
3.13: Drop-weight impact for axial impact test and the test setup prior testing.	65
3.14: Test setup for oblique dynamic test; (a) 20° steel wedge, (b) steel ring secured to the wedge and (c) specimen secured to the 20° steel wedge via a steel ring and mounted on top of load cell.	66
3.15: Rig set-up for oblique impact test.	66
4.1: Force-deformation curves for experimental and FE analysis for (a) empty straight, (b) foam-filled straight, (c) empty conical and (d) foam-filled conical aluminium tubes.	69
4.2: Comparison between experimental and FE results for (a) energy absorption, (b) peak force and (c) length of deformation of aluminium tubes.	70
4.3: Deformation mode of experimental and FE results (a) foam-filled straight and (b) foam-filled conical tubes.	71
4.4: Comparison of force-deformation curve of foam-filled conical tubes subjected to dynamic axial loading at NUS and UoL.	72
4.5: Force-deformation curves for experimental (----) and FE analysis (—) for (a) empty straight, (b) foam-filled straight, (c) empty conical and (d) foam-filled conical aluminium tubes.	73
4.6: Comparison between experimental and FE results for (a) energy absorption, (b) peak force and (c) length of deformation of aluminium tubes.	75

4.7: Deformation mode of experimental and FE results (a) foam-filled straight (b) foam-filled conical tubes.	76
5.1: Effect of filler density on (a) mean force-deformation curves of straight and conical ($\alpha = 5^\circ$ and 10°) aluminium tubes ($D_b = 80$ mm, $t = 0.5$ mm, $L = 160$ mm).	81
5.2: Deformation mode of straight and conical ($\alpha = 5^\circ$ and 10°) aluminium tubes under dynamic axial loading	82
5.3: Effect of filler density on initial peak force of of aluminium straight and conical ($\alpha = 5^\circ$ and 10°) tubes ($D_b = 80$ mm, $t = 0.5$ mm, $L = 160$ mm).	84
5.4: Force-deformation response of empty and foam-filled conical (5°) aluminium tubes with various length ($D_b = 80$ mm, $t = 0.5$ mm).	85
5.5: Effect of filler density on energy histories of straight and conical ($\alpha = 5^\circ$) aluminium tubes with varying length ($D_b = 80$ mm, $t = 0.5$ mm).	86
5.6: Deformed shape of aluminium tubes at 60 mm deformation length with varying length ($D_b = 80$ mm, $t = 0.5$ mm).	87
5.7: Effect of filler density on initial peak force of aluminium tubes with varying length ($D_b = 80$ mm, $t = 0.5$ mm).	88
5.8: Effect of filler density on mean force-deformation histories of conical ($\alpha = 5^\circ$) aluminium tubes with varying bottom diameter ($t = 0.5$ mm, $L = 160$ mm).	89
5.9: Initial peak force as functions of filler density for conical ($\alpha = 5^\circ$) aluminium tubes with varying bottom diameter ($t = 0.5$ mm, $L = 160$ mm).	90
5.10: Effect of filler density on mean force-deformation curves of empty and foam-filled tubes with varying thickness ($D_b = 69.3$ mm, $L = 100$ mm).	91
5.11: Initial peak force as functions of filler density for aluminium tubes with varying thickness ($D_b = 69.3$ mm, $L = 100$ mm).	92
5.12: Deformed shape for empty and foam-filled conical aluminium tubes at 60 mm deformation length with varying thickness ($D_b = 69.3$ mm, $L = 100$ mm).	93
5.13: Effect of filler density on mean force of carbon steel and aluminium ($\alpha = 0^\circ$ and 5°) tubes ($D_b = 80$ mm, $t = 0.5$ mm, $L = 160$ mm).	94
5.14: Effect of filler density on initial peak force of carbon steel and aluminium ($\alpha = 5^\circ$ and 10°) tubes with varying tube material ($D_b = 80$ mm, $t = 0.5$ mm, $L = 160$ mm).	95

5.15: Deformed profiles for straight ($a = 0^\circ$) and conical ($a = 5^\circ$) carbon steel tubes at 70 mm deformation length.	96
5.16: Effect of filler density on SEA-deformation curves of aluminium and carbon steel tubes ($L = 160$ mm, $D_b = 80$ mm, $t = 1.0$ mm).	98
5.17: Critical effective points of aluminium and carbon steel tubes. Dotted line (-----) refers to 80 mm of effective deformation length.	100
5.18: Effect of filler density on empty and foam-filled aluminum and carbon steel tubes: (a) <i>SEA</i> and (b) initial peak force ($L = 160$ mm, $D_b = 80$ mm, $t = 0.5$ mm), (c) <i>SEA</i> and (d) initial peak force ($L = 160$ mm, $D_b = 80$ mm, $t = 1.0$ mm), (e) <i>SEA</i> and (f) initial peak force ($L = 160$ mm, $D_b = 160$ mm, $t = 0.5$ mm), (g) <i>SEA</i> and (h) initial peak force ($L = 160$ mm, $D_b = 240$ mm, $t = 0.5$ mm).	105
5.19: Effect of filler density on initial peak force of conical ($a = 5^\circ$) aluminium tubes with varying load angle ($D_b = 80$ mm, $t = 0.5$ mm, $L = 160$ mm).	110
5.20: Mean force-deformation for empty and foam-filled conical ($a = 5^\circ$) aluminium tubes under dynamic oblique loading.	111
5.21: Mean force-deformation response for straight ($a = 0^\circ$) and conical ($a = 5^\circ$) tubes subjected to various loading conditions.	112
5.22: Initial peak force-deformation response for straight $a = (0^\circ)$ and conical ($a = 5^\circ$) aluminium tubes under oblique loading ($D_b = 80$ mm, $t = 0.5$ mm, $L = 160$ mm).	113
5.23: Deformed profile for empty and foam-filled aluminium tubes with varying semi apical angle at 70 mm deformation length under oblique loading ($D_b = 80$ mm, $t = 0.5$ mm, $L = 160$ mm).	115
5.24: Force-deformation response for (a) empty and (b) foam-filled aluminium tubes of 100 mm and 160 mm length of tubes.	116
5.25: Mean force-deformation response for straight and conical ($a = 5^\circ$) aluminium tubes with various length on (a) force deformation curves and (b) energy absorption capacity ($D_b = 80$ mm, $t = 0.5$ mm).	117
5.26: Deformation mode for straight and conical ($a = 5^\circ$) aluminium tubes at 50 mm deformation length under oblique loading ($D_b = 80$ mm, $t = 0.5$ mm).	118
5.27: Mean force response for conical ($a = 5^\circ$) aluminium tubes for various bottom diameters ($L = 160$ mm, $t = 0.5$ mm) at 60 mm deformation length.	119
5.28: Initial peak force response of conical ($a = 5^\circ$) aluminium tubes as the function of filler density for different bottom diameters.	120

5.29: Deformed profiles for empty and foam-filled ($\alpha = 5^\circ$) conical aluminium tubes at 70 mm deformation length.	121
5.30: Effect of filler density with various thickness on mean-deformation of conical ($\alpha = 5^\circ$) aluminium tubes under dynamic oblique loading ($D_b = 80$ mm, $L = 160$ mm).	122
5.31: Initial peak force for conical ($\alpha = 5^\circ$) conical aluminium tubes with varying thickness.	123
5.32: Force deformation histories of aluminium and carbon steel ($\alpha = 0^\circ$ and 5°) tubes ($D_b = 80$ mm, $t = 0.5$, $L = 160$ mm).	124
5.33: The initial peak force response of conical ($\alpha = 5^\circ$) carbon steel and aluminium tubes ($D_b = 80$ mm, $t = 0.5$, $L = 160$ mm).	125
5.34: Deformed profile of empty and foam-filled carbon ($\alpha = 5^\circ$) steel tubes at 70 mm deformation length ($D_b = 80$ mm, $t = 0.5$, $L = 160$ mm).	126
5.35: Critical effective points of aluminium and carbon steel tubes ($D_b = 80$ mm, $t = 0.5$ mm, $L = 160$ mm).	128
5.36: Critical effective points with varying bottom diameter and thickness. Dotted line (-----) refers to 80 mm of effective deformation length.	130
5.37: Effect of filler density on empty and foam-filled aluminum and carbon steel tubes: (a) <i>SEA</i> and (b) initial peak force ($L = 160$ mm, $D_b = 80$ mm, $t = 0.5$ mm), (c) <i>SEA</i> and (d) initial peak force ($L = 160$ mm, $D_b = 160$ mm, $t = 0.5$ mm), (e) <i>SEA</i> and (f) initial peak force ($L = 160$ mm, $D_b = 160$ mm, $t = 1.0$ mm) and (g) <i>SEA</i> and (h) initial peak force ($L = 160$ mm, $D_b = 240$ mm, $t = 0.5$ mm).	134
6.1: Quadratic RS of (a) <i>SEA</i> and (b) initial peak force for impact velocity of 6 m/s under dynamic axial loading.	148
6.2: Quadratic RS of (a) <i>SEA</i> and (b) initial peak force for impact velocity of 20 m/s under dynamic axial loading.	149
6.3.: Quadratic RS of <i>SEA</i> and initial peak force for impact velocity of 6 m/s under dynamic oblique loading.	161
6.4: Quadratic RS of <i>SEA</i> and initial peak force for velocity of 20 m/s under dynamic oblique loading	162

LIST OF ABBREVIATIONS

WHO	World Health Organization
DOE	Design of experiments
ANOVA	analysis of variance
RS	Response surface
CCD	Central Composite Design
AR	Orthogonal Array
BBD	Box-Behnken Design
FE	Finite element
RSM	Response Surface Methodology
AA6061-T6	Aluminium Alloy 6061-T6
MIROS	Malaysian Institute of Safety Research
KKR	Ministry of Works Malaysia
ASEAN NCAP	ASEAN New Car Assessment Programme
ROPS	Rollover Protective Structures
VFPS	Vehicle Frontal Protection Systems
CPU	central processing unit
UoL	University of Liverpool
NUS	National University of Singapore
ASTM	American Society for Testing and Materials
LWA	Linear Weighted Average

LIST OF SYMBOLS

SEA	Specific Energy Absorption
D, q	Cowper-Symonds material constant
γ, α_2, β	material constant in yield stress calculations
D_o	diameter
D_b	bottom diameter
t	thickness of tube
T	time
ΔT	time step
a	semi apical angle
L	length of tube
b	regression coefficient
θ	load angle
η_c	centre point
\hat{f}	response surface approximation of actual response function
f^*	actual response function
R^2	coefficient of correlation in least square fitting
R_{adj}^2	adjusted coefficient of correlation in least square fitting
$RMSE$	root mean square error in analysis of variance calculations
SSE	sum of squared error in analysis of variance calculations
SST	sum of total squares in analysis of variance calculations
Φ	yield function

δ	length of deformation
δ_{\max}	effective deformation length
ν^p	Poisson's ratio
M	mass
E	Young's Modulus
E_δ	absorbed energy
σ_p	plateau stress
σ_m	mean stress
σ_e	effective Von Mises stress
σ_o^d	dynamic flow stress
σ_o	associated flow stress
σ_y	yield stress
$\bar{\sigma}$	equivalent stress
ρ_f	foam density
ρ_m	mesh density
ρ_{fo}	density of base material
α	shape of yield surface
F_m	mean force
F	instantaneous force
ε	engineering strain
$\dot{\varepsilon}$	plastic strain rate
ε_D	densification strain
$\bar{\varepsilon}$	equivalent strain

ε_{true}	true strain
σ_{true}	true stress
SEA^*	ideal optimum solution of SEA
F^*	ideal optimum solution of initial peak force
V	velocity
w	weighting coefficient
L_e	element length
c	speed of sound
e	statistical error
k	number of variables
c_s	side width
m	number of design sampling points
p	number of non-constant

© This item is protected by original copyright

Penghancuran Tiub Kon Aluminium Diisi Busa Terhadap Bebanan Paksi dan Serong Dinamik

ABSTRAK

Kajian ini dijalankan dengan matlamat untuk menyelidiki tindakbalas tiub kon aluminium terhadap bebanan paksi dan serong dinamik. Kesan pengisian busa terhadap penyerapan tenaga untuk perubahan geometri, bahan tiub dan ketumpatan pengisi dinilai dan dibincangkan. Kajian ini menggunakan model unsur terhingga tak lurus yang telah disahkan dengan data eksperimen. Pola utama yang ditunjukkan oleh keputusan eksperimen telah berjaya diperolehi dalam keputusan unsur terhingga untuk bebanan paksi dan serong dinamik. Walau bagaimanapun, didapati terdapat perbezaan antara keputusan eksperimen dan unsur terhingga terhadap bebanan serong adalah sehingga 35.4 % terutamanya untuk tenaga yang diserap. Perbezaan ini berkemungkinan disebabkan oleh ketebalan yang tidak seragam dan ketidakmampuan untuk mengekang pergerakan tiub pada hujung yang ditetapkan (seperti dalam simulasi) ketika eksperimen. Model yang telah disahkan kemudiannya digunakan untuk menaksir faedah pengisian busa terhadap perubahan geometri, bahan tiub dan ketumpatan pengisi. Pengenalpastian titik efektif kritikal yang mana mewakili jumlah jisim tiub kritikal dan ketumpatan pengisi kritikal di samping pendekatan yang diambil dalam merubah sudut dan mengekalkan diameter bawah dalam keadaan malar terbukti meningkatkan Tenaga Penyerapan Spesifik (*SEA*) tiub diisi busa berbanding tiub kosong. Walau bagaimanapun, pendekatan ini hanya tergunapakai kepada gabungan parameter geometri, bahan tiub dan ketumpatan pengisi yang tertentu sahaja. Manakala, *SEA* tiub yang diisi didapati telah kehilangan prestasi pada 240 mm diameter bawah. Tambahan pula, *SEA* maksimum tidak semestinya dapat dicapai apabila *SEA* tiub diisi meningkat melebihi tiub kosong. Penemuan ini menegaskan betapa pentingnya pemilihan parameter yang bersesuaian seterusnya menunjukkan bahawa parameter ini dapat dikawal dan membolehkan lesapan yang lebih berkesan oleh penyerap tenaga dan bermanfaat untuk aplikasi hentaman. Dengan tujuan untuk mencapai peningkatan prestasi tiub kon aluminium diisi busa, pengoptimuman berbilang-objektif telah dikaji untuk mencapai fungsi berbilang objektif iaitu *SEA* dan puncak daya mula di bawah pelbagai bebanan. Didapati bahawa tiub aluminium yang lurus dan diisi busa lebih berkemampuan untuk mencapai rekabentuk optimum di bawah bebanan paksi dinamik sementara tiub kon kosong lebih berkelebihan di bawah bebanan serong dinamik. Maklumat yang diperolehi menyediakan asas untuk peningkatan penyerap tenaga aluminium di masa hadapan.

Dynamic Axial and Oblique Crushing of Foam-filled Aluminium Conical Tubes

ABSTRACT

The aim of this study was to investigate the response of conical aluminium tubes subjected to dynamic axial and oblique loading. The effect of foam filling on the energy absorption for variation in geometry, tube material and filler density was evaluated and discussed. This study employs a nonlinear finite element model which was validated against experimental data. Main trends in the experimental results are well captured by the FE results under dynamic axial and oblique loading. Nevertheless, the differences observed under oblique loading between experimental and FE results are as high as 35.4 % particularly for energy absorption. These differences may due to uneven thickness and inability to constraint the movement of the tube at the fixed end (as per simulation) during experiment. The validated model was subsequently used to assess the beneficial of foam filling with respect to the variation of geometry, tube material and filler density. The identification of critical effective point which signifies the critical total tube mass and critical filler density with the approach taken in varying the semi apical angle and by keeping the bottom diameter constant proved to enhance the Specific Energy Absorption (*SEA*) of foam-filled tube over that of empty tube. However, these approaches apply to only particular combination of geometrical parameters. Moreover, *SEA* of foam-filled tubes is found to loss its performance at a bottom diameter of 240 mm. On top of this, the maximum *SEA* is not necessarily obtained with achieving higher *SEA* of foam-filled tube over that of empty tube. These findings highlight the importance of appropriate selection of these parameters thus showing that these parameters can be controlled and hence permits an efficient dissipation of energy absorber which is beneficial for impact applications. With the intention of achieving enhanced performance foam-filled conical aluminium tube, multi-objective optimization is explored to search for multiple objective functions namely *SEA* and initial peak force under various loading. It is found that foam-filled straight aluminium tube is favoured in achieving optimum design under dynamic axial loading whilst empty conical tube is preferable under dynamic oblique loading. The information gained serves as a basis for future enhancement of aluminium tube energy absorber.

CHAPTER 1

INTRODUCTION

1.1 Introduction

The growth in population and economy has led to an increase in traffic worldwide. The number of vehicles has continuously increasing from year to year hence increases the number of traffic accidents. In 2010, road accidents are one of the leading causes of death in the world (World Health Organization, 2013).

In Malaysia, according to The Malaysian Institute of Road Safety Research [MIROS] (2014), a total of 462 423 road traffic accidents were reported in 2012, leading to 6 917 fatalities. Projections show that, road traffic death will increase substantially to 8 760 fatalities in 2015 and by 2020, road traffic death is predicted to be 10 716 (MIROS, 2012). Figure 1.1 shows the breakdown of road traffic accidents for road users in 2012 (Ministry of Works Malaysia [KKR], 2013). It is shown that cars account for 30.5 % of the total accidents.

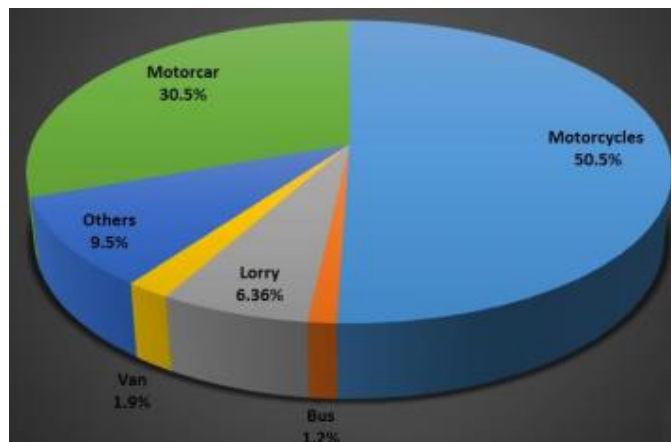


Figure 1.1: Total road traffic accidents in Malaysia for the year of 2012 (*Road Safety Situation In Malaysia, 2013*).

Various factors may contribute to those numbers. Human error, road infrastructures and vehicle conditions are among factors causing road accidents. Despite all these factors, they are preventable. The enhancement of infrastructures and the motor vehicles become the main focus in crashworthiness study nowadays. Crashworthiness refers to the quality of response of a structure during an impact to protect the system under consideration. For motor vehicle, improving crashworthiness may as important as the needs for lighter vehicles as mass reduction allows higher fuel efficiency at minimum cost. However, increasing the safety and achieving mass reduction are two criteria that unquestionably conflict each other. Therefore, extensive research and development in design geometry and applications of new materials seem to be the alternatives to satisfy these constraints.

1.2 Thin-walled tubes and foam as energy absorbers

In vehicle crashworthiness, the enhancement work focuses in several aspects; crash avoidance technology, structural crashworthiness and occupants protection devices. For structural crashworthiness, the application of a collapsible energy absorber allows an undesirable response during an impact to be dissipated in a controlled manner. During impact, the kinetic energy is converted into internal energy or strain energy through plastic deformation whilst at the same time preventing permanent deformations into the rest of the vehicle components. Hence protect the system under consideration. For vehicle, collapsible energy absorber or also known as crash box is connected to the bumpers, located in the front and rear end of the body structure (Reyes, Langseth, & Hopperstad, 2003). However, an energy absorber structure is rarely subjected to pure axial or pure bending loads, but rather a combination of both in

real impact event. In such condition, it will be likely to deform in a combination of axial and global bending modes.

Various structures have been developed and continuously being investigated such as cellular materials, sandwich, lattice structures, composites and thin-walled tubes. Among these structures, thin-walled tubes have been widely used as energy absorber in multidisciplinary fields including automotive and shipping industries due to their impact energy-absorbing capability and manufacturability. The potential of thin-walled tube is further explored by investigating the influence of geometrical and loading parameters on its energy absorption capacity.

Previous studies have shown that tapered and conical tubes would have more stable force-deformation curve under quasi-static and dynamic loading (Mamalis, Manolakos, Ioannidis, & Kostazos, 2005; Nagel & Thambiratnam, 2004; Reid & Reddy, 1986b). Therefore, it is considered preferable than that of straight tube. In addition to that, the introduction of taper and semi apical angle to the straight tubes minimises the chances of collapse by global buckling under oblique loading (Ahmad, Thambiratnam, & Tan, 2010; Nagel & Thambiratnam, 2006). As is seen in Fig. 1.2, conical tube has been applied as an energy absorber by Peugeot for 3008 model in 2011 (Peugeot, March 2014). The two conical energy absorbers have been positioned between the car beam and the chassis leg for energy absorption enhancement and in order to achieve deformation in more controlled manner.

In addressing the mass reduction as part of crashworthiness goal, a combination of cellular material and thin-walled tubes seems advantageous to further improve the energy absorption capacity of thin-walled tubes. Foam is an example of cellular material that demonstrates good energy absorption capacity. It exhibits an almost constant stress plateau and a long stroke of deformation (Lu & Yu, 2003). Honeycombs,

polyurethane, polystyrene and metal foams can be suitable as fillers in thin-walled tubes.



Figure 1.2 : Introduction of Boge impact absorber to Peugeot 3008 model (Peugeot, March 2014).

In order to further improving the energy absorption capacity of thin-walled tubes, extensive investigations have been carried out on the response of foam-filled tubes, numerically and experimentally. The energy absorption has notably increased under quasi-static and dynamic loading particularly when filling the tubes with metallic foam (Seitzberger, Rammerstorfer, Gradinger, & Degischer, 2000; Zhang, Feng, & Zhang, 2010). The increase in energy absorption is due to interaction effect which occurs between the filler and the tube wall, and the strength of the filler itself contributes to the stability of the structure. The interaction effect occurs when the impingement of the tube wall into the filler results in additional compression to the filler. Furthermore, the mode of deformation of foam-filled tube shows a greater tendency to shift from diamond to concertina mode (Güden & Kavi, 2006; Yamada, Banno, Xie, & Wen, 2005). For the same length of deformation, foam-filled tubes